

# AddressVLM: Cross-view Alignment Tuning for Image Address Localization using Large Vision-Language Models

Shixiong Xu<sup>1,2†</sup>, Chenghao Zhang<sup>3†</sup>, Lubin Fan<sup>3\*</sup>, Yuan Zhou<sup>1,2</sup>,  
Bin Fan<sup>4</sup>, Shiming Xiang<sup>1,2</sup>, Gaofeng Meng<sup>1,2,5\*</sup>, Jieping Ye<sup>3</sup>

<sup>1\*</sup>State Key Laboratory of Multimodal Artificial Intelligence Systems,  
CASIA, Zhongguancun East Road, Beijing, 100190, China.

<sup>2</sup>School of Artificial Intelligence, University of Chinese Academy of  
Sciences, Beijing, 100190, China.

<sup>3</sup>Alibaba Cloud, Beijing, 100020, China.

<sup>4</sup>School of Intelligence Science and Technology, University of Science  
and Technology, Beijing, 100190, China.

<sup>5</sup>CAIR, HK Institute of Science & Innovation, Chinese Academy of  
Sciences, HongKong, Country.

\*Corresponding author(s). E-mail(s): [lubin.flb@alibaba-inc.com](mailto:lubin.flb@alibaba-inc.com);  
[gfmeng@nlpr.ia.ac.cn](mailto:gfmeng@nlpr.ia.ac.cn);

Contributing authors: [xushixiong2020@ia.ac.cn](mailto:xushixiong2020@ia.ac.cn);  
[zhangchenghao2018@ia.ac.cn](mailto:zhangchenghao2018@ia.ac.cn); [zhouyuan2023@ia.ac.cn](mailto:zhouyuan2023@ia.ac.cn); [bin.fan@ieee.org](mailto:bin.fan@ieee.org);  
[smxiang@nlpr.ia.ac.cn](mailto:smxiang@nlpr.ia.ac.cn); [yejieping.ye@alibaba-inc.com](mailto:yejieping.ye@alibaba-inc.com);

<sup>†</sup>These authors contributed equally to this work.

## Abstract

Large visual language models (LVLMs) have demonstrated impressive performance in coarse-grained geo-localization at the country or city level, but they struggle with fine-grained street-level localization within urban areas. In this paper, we explore integrating city-wide address localization capabilities into LVLMs, facilitating flexible address-related question answering using street-view images. A key challenge is that the street-view visual question-and-answer (VQA) data provides only microscopic visual cues, leading to subpar performance in fine-tuned models. To tackle this issue, we incorporate perspective-invariant satellite images as macro cues and propose *cross-view alignment tuning* including

a satellite-view and street-view image grafting mechanism, along with an automatic label generation mechanism. Then LVLM’s global understanding of street distribution is enhanced through cross-view matching. Our proposed model, named *AddressVLM*, consists of two-stage training protocols: cross-view alignment tuning and address localization tuning. Furthermore, we have constructed two street-view VQA datasets based on image address localization datasets from Pittsburgh and San Francisco. Qualitative and quantitative evaluations demonstrate that AddressVLM outperforms counterpart LVLMs by over 9% and 12% in average address localization accuracy on these two datasets, respectively.

**Keywords:** Image address localization, Vision-language model, Cross-view alignment

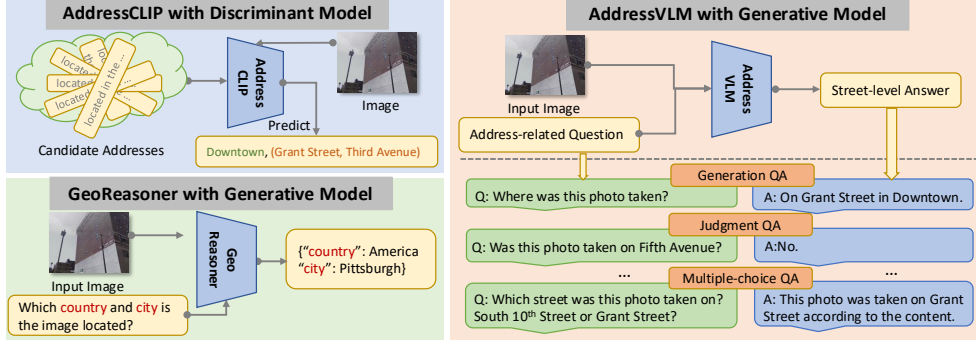
## 1 Introduction

Visual place recognition (VPR) aims to predict the geographic location of a given image, which can be categorized into two types: image geo-localization [1–3] and image address localization [4]. The emergence of Large Vision-Language Models (LVLMs), such as GPT-4V [5], Qwen-VL [6], and LLaVA [7], have significantly impacted various tasks related to images and languages. As generative models capable of generating natural language, they demonstrate enhanced adaptability and flexibility in the image localization task [8]. This proficiency stems from the extensive exposure to street-view and landmark images during their training phases.

Recent work, GeoReasoner [9], integrates a large vision-language model with human inference knowledge for street view geo-localization with reasoning, presenting significant advantages in coarse-grained localization at the country or city level. However, when it comes to address localization for specific districts (*i.e.*, Downtown) or streets (*i.e.*, Fifth Avenue) within a city, it may struggle to predict accurate textual address, since street-view images are more similar and difficult to distinguish and the street-level address names have not been adequately correlated with the corresponding street-view images. In contrast, the previous work AddressCLIP [4] explores city-wide address localization by contrastive learning between street-view images and textual address. Nevertheless, this approach is inherently limited due to its reliance on a discriminative model that can only make distinctions among a constrained set of candidate addresses. As a result, it lacks the flexibility to provide versatile address descriptions and answer other related inquiries.

To combine the advantages of previous work, in this study, we explore how to integrate street-level address localization capabilities into an LVLM. The model is expected to respond flexibly to user inquiries about address localization. We name our model *AddressVLM*, which is designed to handle address-related questions and provide answers accurate to the district and street level. Fig. 1 shows the comparisons of the proposed AddressVLM with AddressCLIP and GeoReasoner. Our method can answer various types of questions including generation, judgment, and multiple-choice.

To realize the above goal, a reasonable approach involves fine-tuning a well-trained LVLM using street-view question-and-answer (VQA) data with LoRA adaptation [10].



**Fig. 1** Comparison of our AddressVLM with AddressCLIP and GeoReasoner. Our approach focuses on city-wide image address localization and flexible address questions and answers related to address using large vision-language models.

However, this straightforward method of *address localization tuning* yields suboptimal performance. The primary reason is that street-view images are sparsely collected in terms of both location and viewpoint, which inhibits the model’s ability to build a global understanding of street distribution across an entire city. Such global information is crucial for effective address localization since street-view images are densely sampled during testing. To supplement the global information in fine-tuning, we introduce perspective-invariant satellite images to establish connections between sparse street-view images. Satellite images are globally consistent and exhibit overlap, allowing for a mapping of the sparse street-view images to a global framework that facilitates inter-image correlations.

Previous research in cross-view geo-localization [11] has shown the viability of correlating satellite images with street-view images. In light of this, we propose a method named *cross-view alignment tuning*, designed to enable LVLMs to align street-view images with street addresses on satellite images annotated with street name labels. This method integrates a global understanding of street distributions within urban environments into LVLMs. It consists of two key components: the satellite-view and street-view image grafting mechanism and the automatic alignment label generation mechanism. The former places street-view images in the upper right corner of their corresponding regional satellite images, serving as the input for cross-view alignment tuning. The latter employs an off-the-shelf LVLm to explain why the street-view image matches the address in the satellite images according to the provided address hint, thus automatically generating labels for the cross-view alignment tuning. By doing this, our full method involves two-stage training protocols: cross-view alignment tuning and address localization tuning.

We introduce two city-wide street-view VQA datasets named Pitts-VQA and SF-Base-VQA, built upon the Pitts-IAL [4, 12] and SF-Base-IAL [4, 13] datasets, respectively. On Pitts-VQA, AddressVLM demonstrates an improvement of 9% compared to the baseline without cross-view alignment tuning. On SF-Base-VQA, AddressVLM achieves an improvement of 12% over the baseline. Moreover, in comparison to the state-of-the-art (SOTA) approach for image address localization using

LVLMS, GeoReasoner [9], our method exhibits improvements of 11% and 14% on the Pitts-VQA and SF-Base-VQA datasets, respectively. The proposed method exhibits excellent city-wide address localization capability compared to general LVLMS. We further provide qualitative results to thoroughly validate the effectiveness of the proposed cross-view alignment tuning strategy. Additional quantitative experiments show that our method can be extended to address localization in multiple cities.

The contributions of this work are summarized as follows: (1) We explore integrating city-wide address localization capabilities into LVLMS to enable flexible address question and answer based on street-view images. (2) We introduce cross-view alignment tuning that integrates the global understanding of urban street distribution into LVLMS, which includes the cross-view image grafting mechanism and the automatic alignment label generation mechanism. (3) We propose AddressVLM that achieves consistent improvements over the baseline and performs superior to the SOTA method GeoReasoner and general LVLMS.

## 2 Related Work

**Visual Place Recognition.** Visual place recognition aims to predict the geographic location of a given image with broad applications in practical scenarios [14]. Most researchers have focused on predicting the latitude and longitude coordinates for input images, known as image geo-localization using retrieval-based methods [2, 3, 15, 16] and classification-based methods [17–20]. Retrieval-based methods involve matching the given image with a database of images tagged with GPS and retrieving the coordinates of the most similar images as the prediction result. Classification-based methods, on the other hand, subdivide the Earth’s surface or cities into geographical cells and predict the geographical unit to which an image belongs. Recent trends have involved leveraging the general text knowledge embedded in visual-language models for geo-localization, including CLIP-based [21] discriminative models such as StreetCLIP [22] with region descriptions and GeoCLIP [23] with GPS information injection, as well as LVLMS-based generative models like GeoReasoner [9] with human reasoning knowledge. However, these models typically focus only on coarse-grained localization at the country or city level. AddressCLIP [4] focus on fine-grained street-level localization within a city, yet this discriminative model is constrained to make distinctions within a limited set of candidate addresses and cannot provide flexible address descriptions or question-and-answer. In this study, we explore integrating fine-grained city-wide address localization capability into LVLMS.

**Large Vision Language Models.** LVLMS has been a new rising research hotspot, which uses powerful Large Language Models (LLMs) [24–27] as a brain to perform vision-language tasks. These general-purpose LVLMS exhibit remarkable effectiveness in visual question-answering tasks [5–7, 28], suggesting a potential path to artificial general intelligence. For VPR, LVLMS can identify the location of input images based on landmarks, Optical Character Recognition (OCR) information, or other notable visual cues, often achieving precision at the level of country or even city [8]. However, the utilization of LVLMS for fine-grained street-level localization remains a challenging issue. This study leverages the capabilities of LVLMS to tackle image address localization in street views.

**Cross-view Geo-localization.** The objective of cross-view geo-localization is similar to VPR, except that its database consists of aerial images instead of ground street views, and the queries might be panorama images. The key challenge is to match features between aerial and ground images in the feature space [11]. A classic approach to tackle this issue is the implementation of Siamese networks for alignment, as suggested by Vigor [29]. To address temporal changes in ground images, the authors in [30] focus on the temporally invariant parts of images. Additionally, some work [31, 32] propose part-based image representation learning to address the orientation and local detail matching issues. Overall, these studies demonstrate the potential for correlating aerial images with street-view images. Inspired by the spirit of cross-view matching, we apply this task to the domain of LVLMs and adapt it to introduce the method of cross-view alignment tuning.

## 3 Method

### 3.1 Problem Statement

The Image Address Localization problem with Visual Question Answering is formalized as follows: given a training dataset  $D_{train} = \{(I_i, Q_i^j, A_i^j)\}_{i=1}^M, j \in [1 \dots N_i]$ , where  $I_i$  represents images and  $(Q_i^j, A_i^j)$  denotes multi-turn questions and answers, our objective is to train a LVLM  $\mathcal{H}_\theta$  to predict answers based on the query images and address-related questions. For each image  $I_i$ , we organize the multi-turn conversation data as a sequence, where the instruction  $S_i^t$  at the  $t$ -th turn as:

$$S_i^t = \begin{cases} [I_i, Q_i^1], & t = 1 \\ Q_i^t, & t > 1 \end{cases} \quad (1)$$

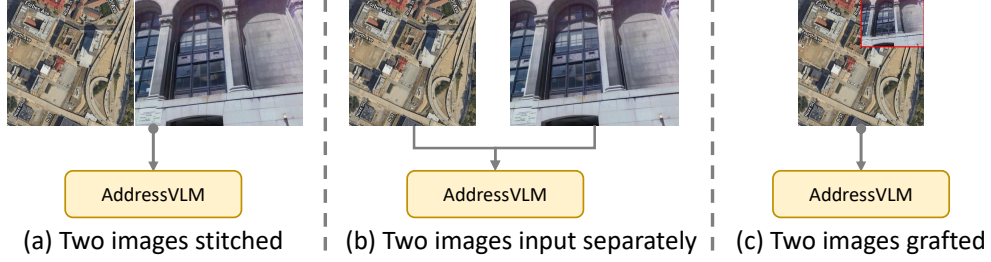
We perform address localization tuning of the LLM on the prediction tokens. Specifically, for a sequence of length  $N$ , we compute the probability of the target answers  $A_i$  by:

$$p(A_i | I_i, S_i) = \prod_{j=1}^N p_\theta(x_j | I_i, S_{<j}, A_{<j}), \quad (2)$$

where  $\theta$  is the trainable model parameters,  $S_{<j}$  and  $A_{<j}$  are the instruction and answer tokens in all turns before the current prediction token  $x_j$ , respectively. In the testing phase, given a query image  $I_k$  and a set of relevant dialogue questions  $Q_j^k$ , the model aims to output the corresponding answers  $A_j^k$  for each question.

### 3.2 Cross-view Alignment Tuning

Street-view images, serving as sparse micro-level visual cues, make it challenging to provide the model with a global macro perspective, which is crucial for effective address localization since street-view images are densely sampled during testing. In contrast, satellite images can be regarded as supplementary macro information, which are perspective-invariant and globally stable to establish connections between sparse street-view images. Inspired by previous works of cross-view matching [11, 33],



**Fig. 2** Three ways of combining the satellite-view and street-view images.

we propose cross-view alignment tuning to align the street-view images with the corresponding street address on satellite images.

**Satellite-view and Street-view Image Grafting.** Multiple methods are available for constructing input images for cross-view alignment tuning, as illustrated in Fig. 2. The first method involves stitching the map and street view images at approximately a 1:1 ratio. This approach appears to preserve the most information from both the map and street view. However, since most LVLMs only accept square-shaped input images (*e.g.*,  $336 \times 336$ ), the necessary padding and resizing operations result in a decreased number of effective visual tokens, which is detrimental to model learning. The second method entails inputting the two images separately. While this strategy allows for maintaining distinct features of both images, it may lead the model to overly rely on the street view content at the expense of the map information. Additionally, this approach effectively doubles the number of visual tokens, negatively impacting training efficiency. To mitigate these issues and encourage the model to focus on the overall street distribution information from the map, while also conforming to the LVLM input size requirements and ensuring training efficiency, we adopt the third method for visual data construction. The size of the map is resized to  $336 \times 336$  to fit the input size of LVLMs.

To address the aforementioned issues of the first two ways, we adopt the satellite-view and street-view image grafting mechanism, where street-view images are scaled down and grafted onto satellite images. Let  $I_{sa}$  and  $I_{st}$  denote the satellite image and street-view image, respectively. The grafting goal is to generate a new image  $I_s$  by combining the two view images. The grafting operation can be expressed as:

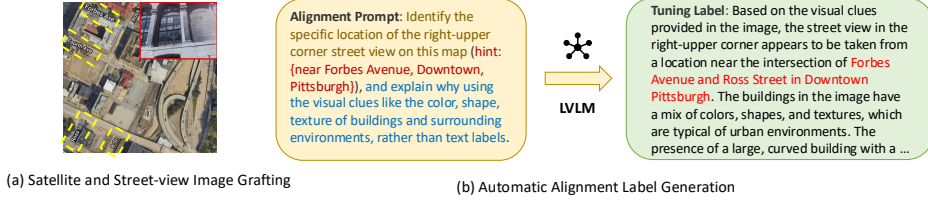
$$I_s = \mathbf{M} \odot I_{sa} + (\mathbf{1} - \mathbf{M}) \odot I_{st}, \quad (3)$$

where  $\mathbf{M}$  denotes a binary mask indicating where to drop out and fill in from two view images,  $\mathbf{1}$  is a binary mask filled with ones, and  $\odot$  is element-wise multiplication. We position the street-view image in the upper right corner of the satellite image, ensuring a longer side overlap ratio  $\delta \in [0, 0.5]$ , as shown in Fig. 3. The text name of each street is marked on the satellite image to facilitate the alignment of street-view images and street addresses, which allows a single image to be used as input. The effects of different grafting parameters is analyzed in Sec. 4.3.

We also provide a comparison of the outcomes for three different grafting methods in Table 1. Comparing the three different grafting methods, our grafting approach

**Table 1** Comparison of the outcomes for three different grafting methods.

Method	$A_d^G$	$A_d^J$	$A_d^M$	$\bar{A}_d$	$A_s^G$	$A_s^J$	$A_s^M$	$\bar{A}_s$	$\bar{A}$	$A_{sd}$
Two image stitched	85.73	92.39	93.42	90.95	67.36	91.05	92.17	85.78	87.91	66.45
Two images input separately	86.52	92.90	94.15	91.33	68.29	90.84	92.71	86.67	88.14	67.39
Two images grafted	88.73	93.54	95.16	92.70	72.51	91.70	93.98	87.46	90.02	69.60



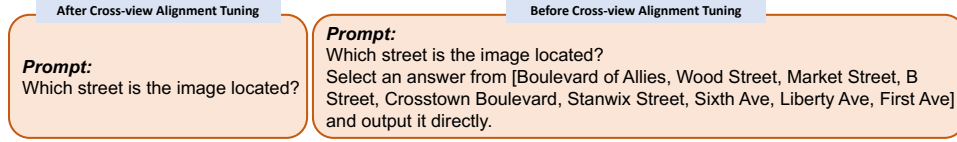
**Fig. 3** Schematic diagram of satellite and street-view image grafting (a), and an example of the alignment prompt and generated label (b). The red and yellow boxes in (a) are only for highlighting and are not marked in the fine-tuning data.

yields the best results. This is attributed to the fact that LLaVA-phi3-mini is designed for single-image input scenarios, creating a significant domain gap when two images are inputted (two images stitched), deviating from its pre-training conditions. Additionally, since CLIP is adapted to square input images, images with a high aspect ratio may lose token information due to resizing and padding operations (two images stitched). In summary, we have chosen the of 0.5 with two images grafted for input image construction.

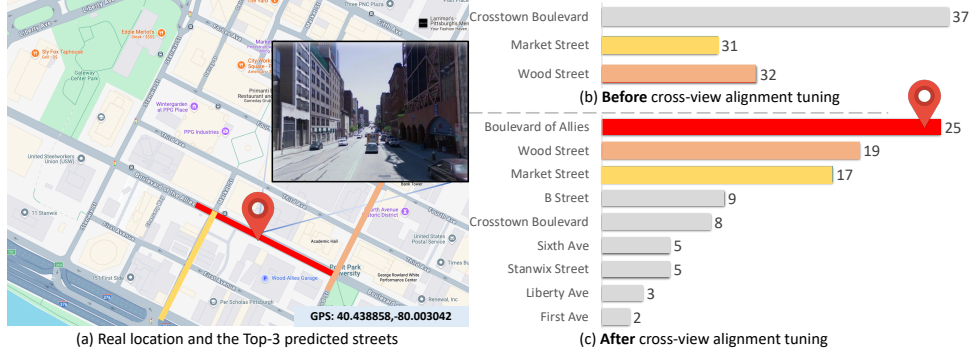
**Automatic Alignment Label Generation.** To enable LVLs to establish a global understanding of urban street layouts using maps, we design a cross-view alignment tuning task. This task allows the model to locate the address of a street-view image by visually matching it with satellite images, where the corresponding textual street name is marked. Meanwhile, we require the model to give the reason for the address prediction. During performing the cross-view alignment tuning task, the model can perceive surrounding street information using OCR capability.

The goal of alignment tuning relies on training the model with appropriate textual labels. An intuitive way is to construct textual labels based on artificial rules and template languages, but this way cannot achieve flexible and diverse descriptions. To this end, we propose an automatic alignment label generation mechanism. In this mechanism, reference answers based on rules are given in advance, and the reasons are generated by a well-trained LVL as textual labels. Here, we provide a *text hint* in the alignment prompt as the standard answer to help generate tuning labels. Fig. 3 shows the pipeline of automatic alignment label generation mechanism with the prompt of label generation. Then, the reference answers are hidden and the alignment tuning is performed using the generated labels. **Discussion.** To demonstrate the effectiveness of the proposed cross-view alignment tuning, we provide qualitative comparisons of the street localization probability distribution before and after the alignment tuning





**Fig. 4** Prompts for models before and after cross-view alignment tuning for qualitative results.



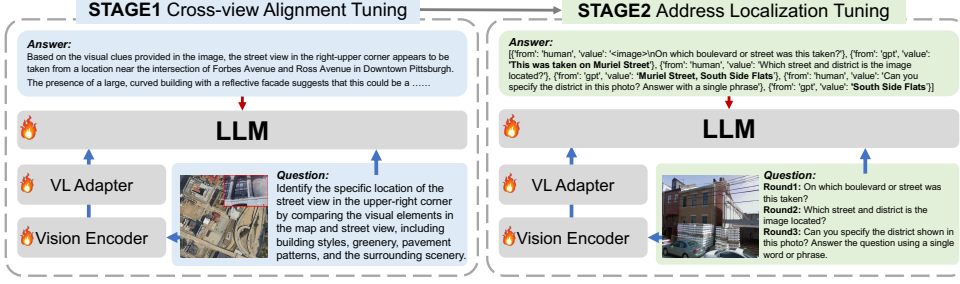
**Fig. 5** Qualitative comparisons of the street localization probability distribution before and after cross-view alignment tuning. We use red, orange, and yellow to represent the top three streets predicted by the model in 100 repeated inferences after alignment fine-tuning, where the length of the color bar represents the number of times the model predicted the corresponding street. The predicted streets are clustered and distributed close to the true location after cross-view alignment tuning. The source map can be found [here](#).

in Fig. 5. Specifically, we set the temperature parameter of LLM to 0.8 to increase inference variability. Then we perform model inference 100 times for each input street-view image with the specific prompt as shown in Fig. 4. For each sample, we record the frequency of each street appearing in the 100 inference results to approximate the model’s understanding of the surrounding street distribution before and after the cross-view alignment tuning. The red marker on the road map indicates the ground truth location of the input image, and the highlighted streets are the Top-3 most frequent outputs. It can be observed that the predicted streets are clustered and distributed close to the ground truth location after cross-view alignment tuning, indicating that the proposed tuning strategy successfully integrates the knowledge of urban street distribution with LVLMs.

### 3.3 Two-stage Training Protocols

**Street-View Visual Question-and-Answer Datasets.** To facilitate our study, we constructed two street-view VQA datasets tailored for address-related QA. These datasets are based on image address localization datasets from Pittsburgh [4, 12] and San Francisco [4, 13]. To enrich the diversity of the QA data, we conceived three QA modes: *generation*, *judgment*, and *multiple-choice*, as shown in Fig.1. The QA data is generated automatically using language templates and is organized through a series of





**Fig. 6** Overview of the proposed framework with two-stages: cross-view alignment tuning and address Localization tuning.

multiple dialogue rounds. We have designated the VQA datasets for two cities as Pitts-VQA and SF-Base-VQA. Specifically, Pitts-VQA contains 10,586 locations with 24 images from different viewpoints for each location and 7 rounds of QA for each image. SF-Base-VQA contains 17,067 locations with 12 images from different viewpoints for each location and 7 rounds of QA for each image. After the labels were manually checked, both datasets are divided into training sets, validation sets, and test sets in a ratio of 7:2:1. We will release them to the community in the future. More details are given in Appendix B.

**Model Architecture.** Fig. 6 illustrates the architecture of the AddressVLM, designed based on the framework established by LLaVA [7]. The model consists of three modules: the Vision Encoder  $g$ , the Vision-Language (VL) Adapter  $h$ , and the Pre-trained LLM  $f$ . For an input satellite-view or street-view image  $I$ , the Vision Encoder provides the visual feature  $Z_v = g(I)$ . The VL Adapter maps the visual features into language embedding tokens, expressed as  $H_v = h(Z_v)$ , where  $H_v \in \mathbb{R}^{N \times D}$  represents refined visual features that are compatible with textual representations. For another input of textual address query  $Q$ , we obtain the embedded tokens from the address query as  $T_v = \Theta(Q)$ , where  $\Theta$  represents the off-the-shelf Tokenizer and Embedding models. Finally, the compressed visual feature sequence and the text sequence are concatenated to feed into the Pre-trained LLM module, represented as  $A = f(H_v, T_v)$ .

The AddressVLM undergoes two stages training: cross-view alignment tuning and address localization tuning. In the first stage, our objective is to integrate the spatial distribution of streets and districts within the entire city into LVLMs through the matching between satellite-view images and street-view images for address localization. This alignment tuning procedure is vital for facilitating the second stage of address localization tuning. In the second stage, we integrate the global prior knowledge of street distribution information to infer the fine-grained, city-wide address location information. Here, we utilize the street-view (VQA) data without satellite-view images. Both stages are fine-tuned using Low-Rank Adaptation (LoRA), which contributes to the overall performance improvements in address localization. This two-stage approach allows the model to better capture complex relationships within the image-address pairs, enhancing its ability to localize addresses accurately by leveraging integrated spatial knowledge.

**Table 2** Performance comparisons with other address localization methods on the Pitts-VQA and SF-Base-VQA datasets.

	Method	$A_d^G$	$A_d^J$	$A_d^M$	$\bar{A}_d$	$A_s^G$	$A_s^J$	$A_s^M$	$\bar{A}_s$	$\bar{A}$	$A_{sd}$
Pitts	LLaVA-Phi3-mini	26.64	60.22	37.81	45.52	0.00	56.23	34.62	36.69	41.01	0.00
	Baseline	84.51	92.72	93.23	90.70	64.31	90.25	91.27	84.00	87.27	60.52
	GeoReasoner	83.29	91.65	91.50	89.41	61.89	89.87	89.68	82.80	86.03	57.78
	<b>AddressVLM</b>	<b>88.73</b>	<b>93.54</b>	<b>95.16</b>	<b>92.70</b>	<b>72.51</b>	<b>91.70</b>	<b>93.98</b>	<b>87.46</b>	<b>90.02</b>	<b>69.60</b>
SF-Base	LLaVA-Phi3-mini	3.78	71.73	42.76	46.89	0.15	52.39	30.85	33.85	40.31	0.00
	Baseline	82.19	93.46	93.14	90.49	65.48	88.25	88.57	82.61	86.51	58.62
	GeoReasoner	81.40	91.07	90.81	88.53	62.89	86.46	84.64	80.08	84.26	55.99
	<b>AddressVLM</b>	<b>86.48</b>	<b>93.72</b>	<b>94.50</b>	<b>92.06</b>	<b>76.09</b>	<b>88.92</b>	<b>92.75</b>	<b>86.66</b>	<b>89.33</b>	<b>70.45</b>

## 4 Experiments

### 4.1 Experimental Setup

**Implementation Details.** AddressVLM is built upon CLIP [21] and Phi-3.1-mini [27] in a LLaVA fashion using the xtuner [34] framework, which is implemented with PyTorch. All images are adjusted to  $336 \times 336$  to fit the input size of the CLIP. More details are provided in Appendix A.

**Evaluation Metrics.** To rigorously assess the model’s address localization capabilities across diverse conversational contexts, we employ various formats and metrics to assess different levels of localization accuracy. We formulate three types of questions: generation, judgment, and multiple-choice. They are applied at both district and street levels. We denote the accuracy for Generation, Judgment, and Multiple-choice question related to district as  $A_d^G$ ,  $A_d^J$ , and  $A_d^M$ , respectively, with their average represented as  $\bar{A}_d$ . Correspondingly, the accuracies for street-level assessments are denoted as  $A_s^G$ ,  $A_s^J$ , and  $A_s^M$ , with an average of  $\bar{A}_s$ . The overall accuracy of both levels localization is represented as  $\bar{A}$ . In addition, we investigate the model’s capability to concurrently generate both street and district information, referred to as  $A_{sd}$ . This metric shares some resemblance to the street-level top-1 accuracy (SA-1) in AddressCLIP [4]. However, it is worth noting that the  $A_{sd}$  we report pertains to generative models, making it a more challenging measure than the discriminative SA-1.

### 4.2 Main Results

**Baselines.** First, we evaluate the adopted pre-trained LVLM to show its zero-shot capabilities for image address localization, denoted by **LLaVA-Phi3-mini**. Subsequently, we reproduce the results of **GeoReasoner** [9] at the district and street levels as the SOTA method. More method details can be found in Appendix C. We conduct only address localization tuning on LLaVA-Phi3-mini, which is referred to as **Baseline** for both methods.

**Comparisons.** Tab. 2 shows the results of our AddressVLM and the aforementioned models on both datasets. Our approach achieves the best results across all metrics on both datasets. Specifically, the zero-shot performance of LLaVA-Phi3-mini is subpar

**Table 3** Ablations study of grafting overlap ratio  $\delta$  and satellite image type for cross-view alignment tuning on two datasets.

Method	$\delta$	Pitts-VQA		SF-Base-VQA	
		$\bar{A}$	$A_{sd}$	$\bar{A}$	$A_{sd}$
Satellite w/o road	0.3	88.36	64.05	87.32	65.33
Satellite	0.3	89.32	68.98	88.67	70.42
Satellite w/o road	0.5	88.06	64.63	87.41	65.93
Satellite	0.5	<b>90.02</b>	<b>69.60</b>	<b>89.33</b>	<b>70.45</b>

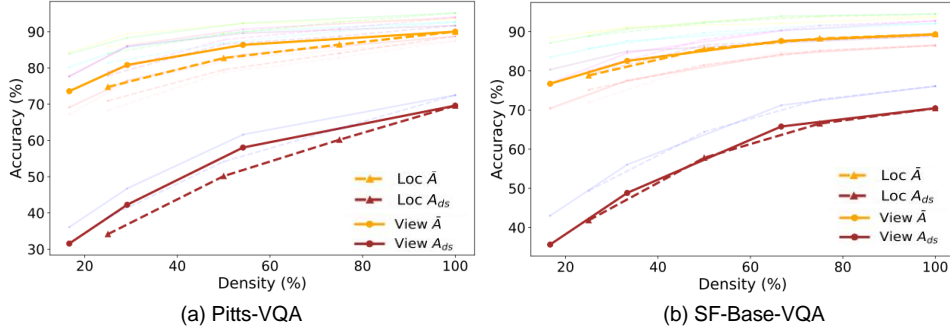
on both datasets, due to its inadequate fine-grained and multi-modal understanding of urban environments. Nevertheless, its performance on  $A_d^J$  is better than random guessing (60.22% vs. 50% and 71.73% vs. 50% on both datasets), suggesting that it does have a foundational level of urban knowledge. After applying our two-stage tuning to LLaVA-Phi3-mini, there is a significant improvement in AddressVLM’s overall performance compared to the zero-shot setting (+49.01% and +49.02% on both datasets in terms of  $\bar{A}$ ). For the SOTA method GeoReasoner, the key lies in the first-stage reasoning tuning that aims at coarse-grained recognition and enhanced reasoning ability. While this strategy yields benefits at the country level, limited distinctions in street scenes within the same city can lead to a detrimental effect, resulting in decreases of 2.74% and 2.63% in terms of  $A_{sd}$  on both datasets. In contrast, our AddressVLM constructs a satellite image and street-view image alignment task in the first-stage tuning, effectively integrating knowledge about street names and global street distribution into the model. Compared to the baseline of directly applying localization tuning, the proposed alignment tuning stage brings significant and consistent performance gains, *e.g.*, +9.08% and +11.83% in terms of  $A_{sd}$  on both datasets. Furthermore, we can observe a performance gap between our AddressVLM and AddressCLIP in terms of street and district localization performance ( $A_{sd}$ ), suggesting that it is still challenging for open-set generative models to achieve comparable results as closed-set classification models in specific tasks. This is a promising direction and we would like to explore it in future work.

### 4.3 Ablation Study

**Grafting Mechanism of Cross-view Alignment Tuning.** The cross-view alignment tuning is a pivotal step for the effectiveness of AddressVLM, with various options for constructing the visual data. The first key factor is the overlap ratio  $\delta$  (default  $\delta = 0.5$ ) of the longer side of the street-view image to the satellite image. The second factor is the type of satellite images, *i.e.*, whether the satellite image is labeled with textual street names. The ablation results about them are shown in Tab. 3. It is shown that reducing  $\delta$  to 0.3 leads to a decline in performance, indicating that small street view images fail to provide sufficient visual details. Meanwhile, removing street labels from satellite images also results in performance degradation since satellite maps inadequately represent street layouts without OCR road information. Therefore, we finally adopt satellite images with street names and set  $\delta = 0.5$ .

**Table 4** Ablation study of training with different parameters during different training phrases, ✓ indicates one module is trainable.

Variants	Stage-1		Stage-2	Pitts-VQA		SF-Base-VQA	
	VE	LLM	VE	$\bar{A}$	$A_{sd}$	$\bar{A}$	$A_{sd}$
A				86.58	63.21	86.74	62.94
B			✓	86.42	62.95	86.31	62.78
C		✓		87.48	63.03	85.92	61.21
D		✓	✓	89.53	66.37	89.63	68.95
E	✓	✓		87.37	63.52	87.07	64.68
Ours	✓	✓	✓	90.02	69.60	89.33	70.45



**Fig. 7** Ablation on different densities of street-view images for address localization on both datasets. The semi-transparent lines in the background are sub-indicators of  $\bar{A}$ , as defined above.

**Training Components in LVLM.** Whether the training parameters in LVLMs are frozen or not usually affects its performance on domain-specific tasks. To this end, we explore the impact of freezing or unfreezing components of AddressVLM in Tab. 4, which includes the Vision Encoder (VE) and LLM. The VLA in both stages and LLM in the second stage are unfrozen by default. Notably, unfreezing the LLM during the first stage yields the most performance improvement. Similarly, unfreezing the VE in the second stage usually achieves better performance than freezing the VE, since the input of the second stage training is street-view images and unfreezing the VE enables the model to better adapt to urban street scenes. Ultimately, unfreezing all parameters leads to the best performance. This result can be attributed to the task’s strong specificity and the availability of a large-scale dataset, which facilitates comprehensive parameter optimization for optimal results [35]. These findings align with previous conclusions in the community.

**Density of Street-view Images.** We investigate the impact of different densities of street-view images used for the address localization tuning, which can be reflected in two aspects: i) The density of viewpoints, meaning how many street views are available for a location (*e.g.*, 100%, 50%, 25%, 12.5%). ii) The density of locations, referring to the down-sampling rate of locations (*e.g.*, 100%, 75%, 50%, 25%). We decouple these factors for separate analysis in Fig. 7. As observed, for viewpoint density, the model

maintains over 88% performance ( $\bar{A}$ ) when the viewpoints are down-sampled to 50%. For location density, the model retains over 71% performance ( $A_{sd}$ ) when locations are down-sampled to 50%. The results indicate that our approach has strong generalization capabilities with lower data densities. Meanwhile, we notice that the sensitivity of our method to viewpoint and location density is similar, which suggests that the density of these two dimensions is equally significance to the localization performance.

**Table 5** Effect of mixed training on both Pitts-IAL and SF-IAL-Base datasets.

Train / Test	District				Street				$\bar{A}$	$A_{sd}$
	$A_d^G$	$A_d^J$	$A_d^M$	$\bar{A}_d$	$A_d^G$	$A_d^J$	$A_d^M$	$\bar{A}_d$		
Pitts / Pitts	88.73	93.54	95.16	92.70	72.51	91.70	93.98	87.46	90.02	69.60
Pitts + SF / Pitts	89.24	93.17	95.16	92.66	72.90	92.77	94.34	88.18	90.37	70.63
SF / SF	86.48	93.72	94.50	92.06	76.09	88.92	92.75	86.66	89.33	70.45
Pitts + SF / SF	87.40	94.24	94.92	92.66	77.05	91.97	93.00	88.48	90.55	71.36

**Scalability for Multiple Cities.** Considering that image address localization may involve multiple cities in practice, we first evaluate the scalability of AddressVLM on both datasets. Specifically, we merge these datasets and train a unified AddressVLM using the proposed two-stage tuning, then evaluate it on both test sets. As shown in Tab. 5, surprisingly, the performance of this unified model surpasses the performance of each separate model slightly on both datasets. We speculate that more cross-view data of the same task facilitates model learning how to locate the street-view image using a map for reference. This finding further demonstrates the scalability of our pipeline, suggesting its potential to extend capabilities across more cities or even an entire country. We further evaluated the performance of our method on datasets outside the United States, specifically in Tokyo, as detailed in Appendix ???. The results show that our method can also achieve good performance, even when the addresses are highly biased. This demonstrates the method’s scalability and adaptability.

**Effect of Mixing General VQA data.** Data mixing is crucial for simultaneously preserving multiple capabilities of the LVLm. To assess the impact of mixing general VQA data on the performance of our approach, we selected the llava\_v1.5\_mix665k VQA dataset as the general data. We mixed it with the stage 2 data in ratios of 5:1 and 1:1, respectively. The results are shown in Table 6. It can be observed that increasing the proportion of address localization VQA data further enhances performance. We believe that by carefully adjusting the data ratio, we can strike a balance between improving the model’s general abilities and its address localization capabilities.

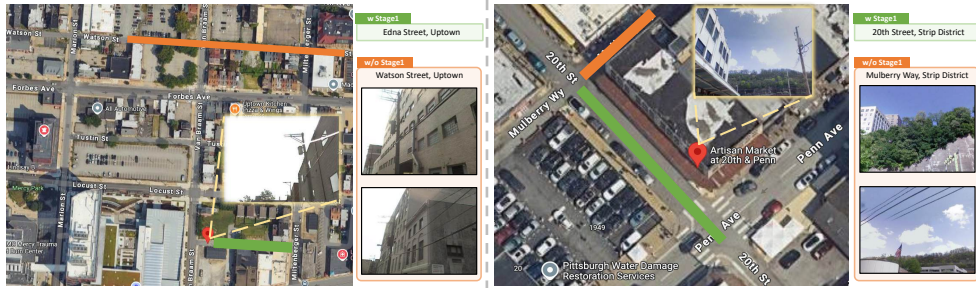
**Performance on Different Backbone.** To validate the generalizability of our method across different backbones, we conducted the same two-stage training using MiniCPM-v2.6, which consists of SigLIP and Qwen2-7B. The results on Pitts-VQA are shown in Table 7. It can be observed that the performance of AddressVLM based on SigLIP and Qwen2-7B is slightly higher than that based on LLaVA-phi3, which demonstrates that adopting a more powerful LVLm can achieve better results.

**Table 6** The results of incorporating different proportions of llava\_v1.5\_mix665k data into our stage 2 training.

Method	$\bar{A}_d$	$\bar{A}_s$	$\bar{A}$	$A_{sd}$
w / llava_v1.5_mix665k (5:1)	84.38	75.70	79.95	42.08
w / llava_v1.5_mix665k (1:1)	87.97	79.08	83.43	50.53
wo / llava_v1.5_mix665k	92.70	87.46	90.02	69.60

**Table 7** Performance on MiniCPM-v2.6, which consists of a vision encoder of SigLIP and an LLM of Qwen2-7B.

Method	$\bar{A}_d$	$\bar{A}_s$	$\bar{A}$	$A_{sd}$
CLIP + Phi3-mini	92.70	87.46	90.02	69.60
SigLIP + Qwen2-7B	93.57	88.58	90.97	70.49



**Fig. 8** Qualitative visualization comparison of the impact of whether using the first-stage cross-view alignment tuning. The street-view images around the mispredicted streets are also depicted.

**Results on Tokyo 24/7.** To validate the effectiveness of our method in cities out of the US, we evaluated it on Tokyo 24/7 dataset. In the Tokyo dataset related to image geolocation tasks, we collected a total of 52080 street view images (from 4340 locations with 12 images for each location), along with 52764 sets of VQA dialogue data and corresponding satellite images for training. The addresses were categorized into two levels: Chome and Street. We completed two stages of fine-tuning, and the results on the test set (7440 images from 1240 locations) are given in Table 8.

As can be seen, our method demonstrated good performance on the Tokyo dataset even if the addresses are highly biased, effectively utilizing Tokyo’s address division system. This underscores the method’s scalability and adaptability in modern cities with the well-defined address-related VQA data.

**More Results about the selection of  $\delta$ .** Table 9 presents the results on Pitts-VQA when  $\delta$  is set to 0.3, 0.5, and 0.7. It can be observed that the results are superior when  $\delta = 0.5$ , it outperforms both  $\delta = 0.3$  and  $\delta = 0.7$ . This is because when  $\delta$  is too small, there is insufficient fine-grained information from the street view images, and when delta is too large, it obscures most of the map area, leading to a lack of information from the map.

**Table 8** Results on Tokyo dataset.

Method	$A_d^G$	$A_d^J$	$A_d^M$	$\bar{A}_d$	$A_s^G$	$A_s^J$	$A_s^M$	$\bar{A}_s$	$\bar{A}$	$A_{sd}$
AddressVLM	73.85	89.49	88.62	84.99	63.52	88.28	86.03	81.57	82.28	65.81
AddressVLM w/o stage1	70.63	86.22	85.93	83.14	58.06	85.39	84.72	78.37	80.76	56.37

**Table 9** Results on Pitts-VQA with more different selection of  $\delta$ .

$\delta$	$A_d^G$	$A_d^J$	$A_d^M$	$\bar{A}_d$	$A_s^G$	$A_s^J$	$A_s^M$	$\bar{A}_s$	$\bar{A}$	$A_{sd}$
0.3	87.32	92.93	94.59	92.05	71.61	91.04	93.27	86.78	89.32	68.98
0.5	88.73	93.54	95.16	92.70	72.51	91.70	93.98	87.46	90.02	69.60
0.7	86.58	92.33	93.86	91.22	70.35	90.49	92.65	85.81	88.49	68.07

#### 4.4 Qualitative Results

**Effectiveness of Cross-view Alignment Tuning.** To demonstrate the effectiveness of the proposed cross-view alignment tuning, we present examples with correct positioning by our model with the alignment tuning, as shown in Fig. 8. We present street-view images that are predicted incorrectly without the first-stage alignment tuning. It can be observed that there exists high degree of similarity between the street views near the mispredicted streets and those of the ground truth streets. This issue is difficult to address by only using the second-stage address localization tuning. In contrast, the first-stage alignment tuning supplements the missing global street information and establishes connections between street-view images, thus helping the model better confirm the location of the street-view image.

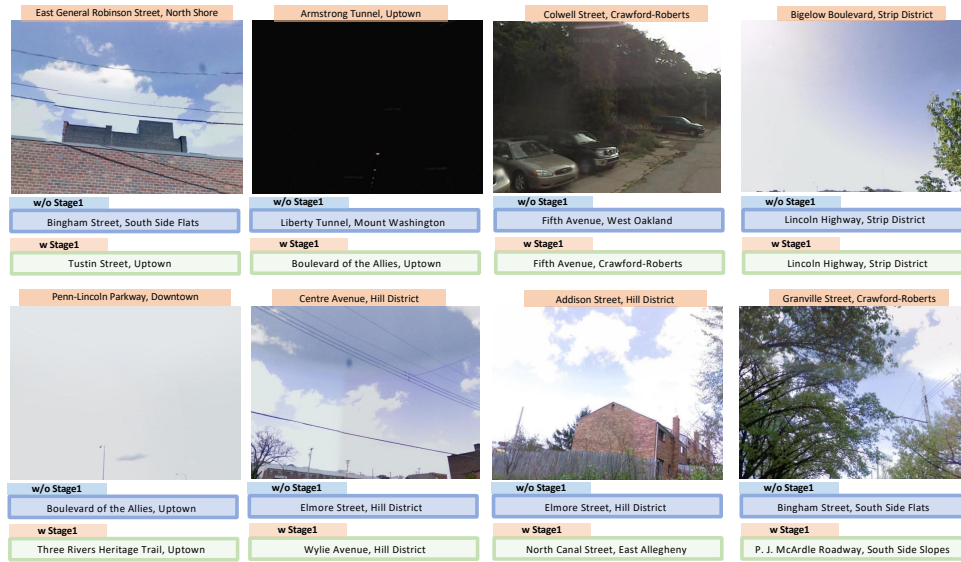
**Case Study.** We demonstrate more examples where AddressVLM accurately locates while the baseline model without cross-view alignment tuning makes errors in localization, as shown in Fig. 9. We also provide some failure cases that both model can not localize correctly in Fig. 9. One can see that these images are of low visual cues, which are difficult to recognize even for human experts.

**Comparisons with General LVLMS.** We further present examples of AddressVLM in real-world inference and provide a comparison with SOTA general LVLMS, *e.g.*, GPT-4o [5], Sonnet 3.5 [36], and Qwen2-VL [6, 37] and LLaVA-Phi3-mini, as shown in Fig. 10. AddressVLM consistently delivers high-quality results across various VQA scenarios. In contrast, the performance of SOTA models is significantly constrained by whether the input images contain sufficient identifiable information, such as street names and landmarks. This demonstrates that with minimal fine-tuning, AddressVLM can achieve a granular understanding of urban environments using only 4B parameters. This ensures its feasibility for future on-device deployment and updates.





(a) Examples where AddressVLM predicts correctly but the Baseline model predicts incorrectly



(b) Failure Cases

**Fig. 9** More examples where AddressVLM accurately locates while the baseline model makes errors in localization (a), as well as failure cases (b).


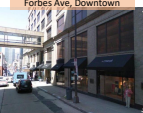



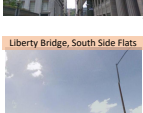
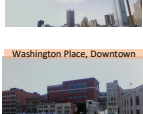



	<p>What district is this photo taken in? Answer the question using a single word or phrase.</p> <p>AddressVLM</p> <p>Crawford-Roberts.</p>	<p>GPT-4o</p> <ol style="list-style-type: none"> <li>1. I cannot determine the ... [Failed]</li> <li>2. I'm unable to identify the specific district based solely on the image provided... [Failed]</li> </ol> <p>Qwen2-VL</p> <ol style="list-style-type: none"> <li>1. downtown. [Surrounding district]</li> <li>2. The photo appears to be taken in an urban or suburban area with a ... [Invalid]</li> </ol> <p>Sonnet</p> <ol style="list-style-type: none"> <li>1. Rust Belt. [Invalid]</li> <li>2. Appalachian city. [City level]</li> <li>3. I don't have enough context to... [Failed]</li> </ol> <p>LLaVA</p> <ol style="list-style-type: none"> <li>1. Rural. [Invalid]</li> <li>2. Hill district. [Surrounding district]</li> <li>3. Downtown. [Surrounding district]</li> </ol>
	<p>What street is this photo taken on? Answer the question using a single word or phrase.</p> <p>AddressVLM</p> <p>Forbes Ave.</p>	<p>GPT-4o</p> <ol style="list-style-type: none"> <li>1. Forbes Avenue.</li> <li>2. Cherry Way [Invalid]</li> <li>3. Smithfield Street [Hallucination]</li> </ol> <p>Qwen2-VL</p> <ol style="list-style-type: none"> <li>1. main. [Hallucination]</li> <li>2. Without specific landmarks or signs, it's difficult to determine the exact street. [Failed]</li> </ol> <p>Sonnet</p> <ol style="list-style-type: none"> <li>1. The street name is not visible in the provided image, so I cannot ... [Failed]</li> <li>2. The street name is not discernible ... [Failed]</li> </ol> <p>LLaVA</p> <ol style="list-style-type: none"> <li>1. Fashion [Invalid]</li> <li>2. Madrid [City level]</li> <li>3. Main [Hallucination]</li> </ol>
	<p>Which street and district is the image located? Answer the question using a single phrase.</p> <p>AddressVLM</p> <p>Second Ave, Downtown</p>	<p>GPT-4o</p> <ol style="list-style-type: none"> <li>1. Holland Tunnel, Manhattan. [Hallucination]</li> <li>2. W 33rd Street, Hudson Yards. [Hallucination]</li> <li>3. West Side Highway, Hell's Kitchen. [Hallucination]</li> </ol> <p>Qwen2-VL</p> <ol style="list-style-type: none"> <li>1. The image is located in the downtown area of a city.</li> <li>2. Hennepin Avenue, Downtown</li> </ol> <p>Sonnet</p> <ol style="list-style-type: none"> <li>1. This appears to be an Urban district.</li> <li>2. The image appears to depict an urban street in a downtown district.</li> </ol> <p>LLaVA</p> <ol style="list-style-type: none"> <li>1. Woodland ave [Hallucination]</li> <li>2. Highway 40 [Invalid]</li> <li>3. I-94 [Invalid]</li> </ol>
	<p>What district is this photo taken in? Answer the question using a single word or phrase.</p> <p>AddressVLM</p> <p>Downtown.</p>	<p>GPT-4o</p> <ol style="list-style-type: none"> <li>1. Philadelphia. [City level]</li> <li>2. Downtown.</li> </ol> <p>Qwen2-VL</p> <ol style="list-style-type: none"> <li>1. downtown.</li> <li>2. Without specific landmarks or more context, it's difficult to pinpoint ... [Failed]</li> </ol> <p>Sonnet</p> <ol style="list-style-type: none"> <li>1. Financial District [Hallucination]</li> </ol> <p>LLaVA</p> <ol style="list-style-type: none"> <li>1. Financial [Invalid]</li> <li>2. Downtown</li> </ol>
	<p>What street is this photo taken on? Answer the question using a single word or phrase.</p> <p>AddressVLM</p> <p>Smithfield Street.</p>	<p>GPT-4o</p> <ol style="list-style-type: none"> <li>1. I am unable to determine the street from this image alone. [Failed]</li> <li>2. I cannot determine the street ... [Failed]</li> </ol> <p>Qwen2-VL</p> <ol style="list-style-type: none"> <li>1. main. [Hallucination]</li> <li>2. The photo is taken on Wall Street.</li> </ol> <p>Sonnet</p> <ol style="list-style-type: none"> <li>1. City street [Hallucination]</li> <li>2. Downtown. [District level]</li> <li>3. The image does not provide enough ... [Failed]</li> </ol> <p>LLaVA</p> <ol style="list-style-type: none"> <li>1. Fifth avenue</li> <li>2. Cross street [Hallucination]</li> <li>3. Main [Hallucination]</li> </ol>
	<p>Which street and district is the image located? Answer the question using a single phrase.</p> <p>AddressVLM</p> <p>Liberty Bridge, South Side Flats</p>	<p>GPT-4o</p> <ol style="list-style-type: none"> <li>1. Fort Pitt Boulevard, Downtown Pittsburgh</li> <li>2. Grant Street, Downtown Pittsburgh.</li> </ol> <p>Qwen2-VL</p> <ol style="list-style-type: none"> <li>1. The image is located in the downtown area of Pittsburgh, Pennsylvania.</li> <li>2. Without specific landmarks ... [Failed]</li> </ol> <p>Sonnet</p> <ol style="list-style-type: none"> <li>1. The image does not provide enough contextual information ... [Failed]</li> </ol> <p>LLaVA</p> <ol style="list-style-type: none"> <li>1. Downtown</li> <li>2. Chicago [City level]</li> <li>3. 13th street [Hallucination]</li> </ol>
	<p>What district is this photo taken in? Answer the question using a single word or phrase.</p> <p>AddressVLM</p> <p>Downtown.</p>	<p>GPT-4o</p> <ol style="list-style-type: none"> <li>1. Downtown.</li> <li>2. Strip District. [Hallucination]</li> </ol> <p>Qwen2-VL</p> <ol style="list-style-type: none"> <li>1. downtown.</li> <li>2. This photo appears to be taken in a city district, likely a downtown ...</li> </ol> <p>Sonnet</p> <ol style="list-style-type: none"> <li>1. Downtown</li> <li>2. Based on the image, this appears to be taken in a downtown ...</li> </ol> <p>LLaVA</p> <ol style="list-style-type: none"> <li>1. Downtown.</li> </ol>
	<p>What street is this photo taken on? Answer the question using a single word or phrase.</p> <p>AddressVLM</p> <p>Miltner Street.</p>	<p>GPT-4o</p> <ol style="list-style-type: none"> <li>1. Sorry, I can't determine the street based on this image. [Failed]</li> <li>2. I cannot determine the street ... [Failed]</li> </ol> <p>Qwen2-VL</p> <ol style="list-style-type: none"> <li>1. main. [Hallucination]</li> <li>2. The photo is taken on a street in an urban area, but the specific street name is ... [Failed]</li> </ol> <p>Sonnet</p> <ol style="list-style-type: none"> <li>1. The street name is not visible in the provided image. [Failed]</li> </ol> <p>LLaVA</p> <ol style="list-style-type: none"> <li>1. Main. [Hallucination]</li> <li>2. This photo is taken on a residential street. [Hallucination]</li> </ol>
	<p>Which street and district is the image located? Answer the question using a single phrase.</p> <p>AddressVLM</p> <p>French Street, Downtown</p>	<p>GPT-4o</p> <ol style="list-style-type: none"> <li>1. 9th Street, Cultural District. [Hallucination]</li> </ol> <p>Qwen2-VL</p> <ol style="list-style-type: none"> <li>1. The image is located in the downtown area of a city.</li> <li>2. Downtown area of Pittsburgh.</li> </ol> <p>Sonnet</p> <ol style="list-style-type: none"> <li>1. Urban street in a downtown area.</li> <li>2. The image appears to be located on a downtown city street.</li> </ol> <p>LLaVA</p> <ol style="list-style-type: none"> <li>1. Chicago [City level]</li> <li>2. Murray st and west 14th st [Hallucination]</li> <li>3. Downtown</li> </ol>
	<p>Which street and district is the image located? Answer the question using a single phrase.</p> <p>AddressVLM</p> <p>Freyburg Street, South Side Flats</p>	<p>GPT-4o</p> <ol style="list-style-type: none"> <li>1. I'm unable to determine the specific street and district based on the image alone. [Failed]</li> <li>2. I cannot determine the specific ... [Failed]</li> </ol> <p>Qwen2-VL</p> <ol style="list-style-type: none"> <li>1. Hill District of Pittsburgh, Pennsylvania.</li> <li>2. The image is located in a residential district, but the specific street ... [Failed]</li> </ol> <p>Sonnet</p> <ol style="list-style-type: none"> <li>1. Unidentified residential street. [Failed]</li> <li>2. residential street in an unnamed district. [Failed]</li> </ol> <p>LLaVA</p> <ol style="list-style-type: none"> <li>1. Santa fe, downtown [Hallucination]</li> <li>2. Rocky hill [Invalid]</li> <li>3. 1st street [Hallucination]</li> </ol>

Fig. 10 Qualitative comparison of address question-answering capabilities with general LVLMS.

## 5 Conclusion

In this work, we propose AddressVLM for city-wide address localization, which can perform flexible address question-answering for street-view images. The core idea is to leverage cross-view alignment tuning between satellite-view images and street-view images to integrate a global understanding of street distribution into LVLm. This contains two key components, namely the satellite and street view image grafting mechanism, and the automatic alignment label generation mechanism. The model undergoes two-stage fine-tuning, including cross-view alignment tuning and address localization tuning. Extensive experiments show that the proposed AddressVLM surpasses general LVLms and SOTA localization LVLms, and can be extended to multiple cities. In future work, we would like to explore cities on different continents and adopt larger LVLms.

**Limitations.** Thanks to the proposed image crafting mechanism, AddressVLM can perform cross-view alignment tuning. The current method is only a preliminary exploration, the relatively low resolution of street view images may affect the LVLm’s ability to understand them. In the future, more sophisticated cross-view image alignment methods are worth studying to further improve performance.

## Appendix A Implementation Details

All our experiments are conducted using the xtuner framework on 8 RTX 3090 GPUs. The torch version is 2.4.0, the CUDA version is 12.1, and the transformers version is 4.37.2. The main hyperparameter settings are given in Tab. A1.

**Table A1** Hyper-parameter settings of the both two tuning stage.

Hyper-parameter	Values
Batch Size	$4 \times 8$
Gradient Accumulation	16
Learning Rate	$1e-5$
Weight Decay	0
Betas	(0.9, 0.999)
Warmup Ratio	0.03
LoRA Rank	128
LoRA Dropout	0.05
Model Max Length	$2048 - (336/14)^2$

## Appendix B Datasets Details

We provide detailed information about the two constructed VQA datasets as a supplementary to Sec. 3.3, listed in Tab. B2. The dataset information includes the number of locations, the number of street view images, and the proportions of various dialogue types in the multi-turn conversations for both Pitts-VQA and SF-Base-VQA datasets.

Generally, the distribution of address question types in the training set is balanced (1:1:1). In the test set, to accommodate both answer types (Yes/No) in judgment questions, we increased the judgment questions for each district-related and street-related question with answers set as "Yes" or "No", respectively. As a result, the proportion of judgment questions is nearly twice that of the generation and multiple-choice questions. Moreover, we provide comparisons between the proposed datasets with existing related datasets in Table B3.

**Table B2** More details of the constructed Pitts-VQA and SF-VQA datasets.

Statistics	Pitts-VQA		SF-Base-VQA	
	Train	Test	Train	Test
Covered Area	20 km <sup>2</sup>	20 km <sup>2</sup>	6 km <sup>2</sup>	6 km <sup>2</sup>
Number of locations	7410	798	11946	1707
Number of Districts	19	19	15	15
Number of Streets	194	165	121	110
Number of images	177840	19152	143352	20484
Number of questions	533520	168409	430056	181943

**Table B3** Comparisons between the proposed datasets with existing related datasets.

Statistics	Pitts-VQA	SF-Base-VQA	Pitts-IAL	SF-IAL-Base	Pitts-250K	SF-XL
Images	178K/19K	143K/21K	234K/19K	184K/21K	250K/24K	41.2M/1K
GPS	Yes	Yes	Yes	Yes	Yes	Yes
Address	Yes	Yes	Yes	Yes	No	No
QA	533K/168K	430K/182K	N/A	N/A	N/A	N/A

Additionally, the question templates for different types of questions and address is given in Tab. B4. Each address type includes 10 distinct templates, resulting in 20 templates in total. Subsequently, different question types are generated by appending different prompts for the three question categories, as shown in Tab. B5. We replace the contents in "[]" with the ground truth location names (*e.g. street and district*) before appending them to the address prompts.

## Appendix C Reproduction of GeoReasoner

The training process for GeoReasoner [9] consists of two stages. The first stage involves coarse-grained localization at the country level, accompanied by intricate reasoning derived from game data. The second stage is centered on fine-grained localization at the city level, utilizing Google Street View data. In our study, we replicate this pipeline to achieve district and street-level localization within the same urban area. A primary distinction between GeoReasoner and our AddressVLM lies in the data employed during the first stage. In the original work of GeoReasoner, the first stage data integrates

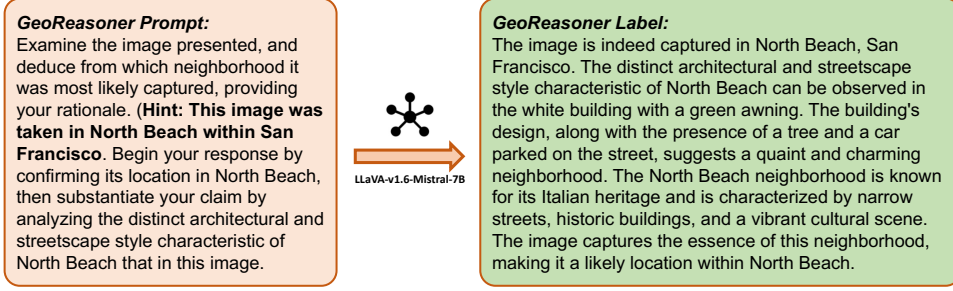
**Table B4** Question Templates for VQA Data Generation.

Address Type	Template
District	<p>Tell me the district where this image was captured.</p> <p>I'm curious about the district, where is this?</p> <p>In which urban district was this photo taken?</p> <p>Can you identify which district this is?</p> <p>What district is shown in this photograph?</p> <p>What major district does the photo fall under?</p> <p>I'm looking for the name of the district in this photo, can you help?</p> <p>Can you specify the district shown in this photo?</p> <p>Which district is depicted in the photo?</p> <p>What's the name of the district shown in the photo?</p>
Street	<p>Identify the street in this image, please.</p> <p>What is the street seen in this picture called?</p> <p>On which boulevard or street was this taken?</p> <p>Give me the name of the street that appears in this photograph.</p> <p>Where was this, can you name the street?</p> <p>What's the name of the avenue or street captured in this shot?</p> <p>The street in this image, what is it named?</p> <p>What's the name of this street shown in the photo?</p> <p>Can you tell me which road this is?</p> <p>What thoroughfare is depicted here?</p>

**Table B5** Appended Prompts to Generate Different Question Types.

Question Type	Template
Generation	Answer the question using a single word or phrase.
Judgement	Is this image taken [On STREET/IN DISTRICT], Yes or No?
Multiple Choice	<p>Which of the following [STREET/DISTRICT] correctly represents the location shown in the image?</p> <p>(A) [OPTION A] (B) [OPTION B] (C) [OPTION C] (D) [OPTION D].</p> <p>Please select the correct option (A/B/C/D).</p>

external knowledge sourced from real geo-localization games. For district-level localization, we generate reasoning data by emulating the reasoning generation pipeline utilized for our cross-view tuning data. An example of the prompt and the generated reasoning label for the first stage of GeoReasoner is presented in Fig. B1. To facilitate a comprehensive comparison across various metrics outlined in Sec. 4.1, we employ the same VQA data for training the second stage of GeoReasoner.



**Fig. B1** An example of the prompt and the generated reasoning label for the first stage of GeoReasoner. The model of LLaVA-v1.6-Mistral-7B is adopted for label generation.

## Appendix D Implementation Details of Qualitative Results

### D.1 Qualitative Results in Sec. 3.2

In Fig. 5, we conduct a quantitative analysis of the cross-view alignment tuning by examining the outputs from two distinct models. While the first stage utilizes grafted images as inputs, our principal objective is to establish a connection between street-view images and the street addresses. Consequently, we employ only street-view images as the input for this analytical evaluation.

**After Cross-view Alignment Tuning.** For discriminative models like CLIP, we can compare the embeddings of street views and address texts to assess whether the model effectively associates street layouts with street views. However, this method is not suitable for the generative models discussed in this study. Instead, we leverage the inherent randomness in the output of generative models. Specifically, we increase the temperature of the model during inference from 0.1 to 0.8 to encourage output variability. By performing inference for 100 times on the same input image, we can count the number of different valid streets, approximating the output distribution for the model for a given input.

**Before Cross-view Alignment Tuning.** Since the image address localization task is quite challenging, the model without any downstream fine-tuning (zero-shot model) struggles to produce valid street outputs directly. Therefore, we organize all the street names generated by the model above into options, allowing the zero-shot model to select one street from this given list for output. The difference between the prompts of these two models is given in Fig. 4.

### D.2 Qualitative results in Sec. 4.4

In Sec. 4.4, we demonstrate the results of four current state-of-the-art proprietary and open-source models on several samples in our datasets. Our AddressVLM is capable of generating outputs as the requirement in the prompt. However, the outputs of other LVLMS are more diverse and uncontrollable. Therefore, for each sample, we conduct multiple inferences (5-10 times) for each input, and display several most frequently responses.



**Table C6** Detailed results of the ablation studies on the complementary metrics.

Ablations		District				Street				$\bar{A}$	$A_{sd}$
		$A_d^G$	$A_d^J$	$A_d^M$	$\bar{A}_d$	$A_s^G$	$A_s^J$	$A_s^M$	$\bar{A}_s$		
Pitts-VQA	Satellite w/o road (0.3)	85.93	93.00	93.70	91.33	67.24	91.18	92.55	85.51	88.36	64.05
	Satellite (0.3)	87.32	92.93	94.59	92.05	71.61	91.04	93.27	86.78	89.32	68.98
	Satellite w/o road (0.5)	86.23	92.42	93.54	91.09	67.97	90.50	91.79	85.17	88.06	64.63
	Variant A	85.57	90.73	92.03	89.77	65.60	89.42	90.39	83.90	86.58	63.21
	Variant B	85.48	90.65	92.12	89.59	65.05	89.21	90.02	83.44	86.42	62.95
	Variant C	84.86	91.98	92.85	90.34	66.39	90.63	91.46	84.75	87.48	63.03
	Variant D	87.36	93.23	95.08	92.66	71.19	91.58	93.85	87.02	89.53	66.37
	Variant E	85.00	92.02	92.65	90.34	66.64	90.27	91.05	84.54	87.37	63.52
	View-4/24	69.14	84.29	83.90	80.21	36.08	77.68	77.71	67.25	73.58	31.55
	View-7/24	76.54	89.38	88.33	85.73	46.75	85.90	86.14	76.13	80.83	42.25
	View-13/24	83.67	92.28	92.34	90.04	61.60	89.58	90.69	82.84	86.36	58.04
	Location-1/4	70.95	85.91	83.97	81.47	38.81	77.91	78.92	68.35	74.76	34.14
	Location-2/4	79.53	89.62	89.40	86.91	54.17	86.59	87.79	78.76	82.74	50.16
	Location-3/4	84.06	92.18	92.69	90.18	63.34	88.73	90.88	82.90	86.46	60.19
AddressVLM	88.73	93.54	95.16	92.70	72.51	91.70	93.98	87.46	90.02	69.60	
SF-Base-VQA	Satellite w/o road (0.3)	84.11	91.82	92.64	90.85	73.59	88.38	90.51	84.57	87.32	65.33
	Satellite (0.3)	85.88	93.10	93.92	91.52	75.27	88.04	92.18	85.79	88.67	70.42
	Satellite w/o road (0.5)	84.39	91.85	92.79	90.88	73.87	88.35	90.68	84.32	87.41	65.93
	Variant A	82.92	92.60	92.41	90.07	69.29	88.27	88.13	83.47	86.74	62.94
	Variant B	82.90	92.50	92.03	89.92	68.90	87.14	87.97	82.77	86.31	62.78
	Variant C	82.05	91.99	92.26	89.51	67.90	87.13	87.53	82.39	85.92	61.21
	Variant D	85.87	94.73	95.16	92.57	74.60	90.22	92.05	86.76	89.63	68.95
	Variant E	83.55	92.25	92.75	90.15	71.28	87.91	89.20	84.06	87.07	64.68
	View-2/12	70.47	88.39	87.11	83.47	43.01	80.31	76.87	70.08	76.71	35.65
	View-4/12	77.52	91.18	90.74	87.57	56.05	84.97	84.54	77.59	82.53	48.83
	View-8/12	84.23	92.11	93.94	90.34	71.20	87.12	90.23	84.74	87.63	64.72
	Location-1/4	75.14	89.77	88.84	85.78	49.39	79.06	80.04	71.95	78.80	41.83
	Location-2/4	81.52	92.69	92.27	89.72	64.42	86.62	88.02	81.49	85.56	57.81
	Location-3/4	85.17	93.85	93.92	91.64	72.70	87.80	91.55	84.94	88.26	66.53
AddressVLM	86.48	93.72	94.50	92.06	76.09	88.92	92.75	86.66	89.33	70.45	

## Appendix E Detailed Results of Ablation Studies

We provide the detailed results of the ablation studies under all the metrics in Tab C6.

## References

- [1] Arandjelovic, R., Gronat, P., Torii, A., Pajdla, T., Sivic, J.: Netvlad: Cnn architecture for weakly supervised place recognition. In: CVPR, pp. 5297–5307 (2016)
- [2] Wang, R., Shen, Y., Zuo, W., Zhou, S., Zheng, N.: Transvpr: Transformer-based place recognition with multi-level attention aggregation. In: CVPR, pp. 13648–13657 (2022)
- [3] Ali-Bey, A., Chaib-Draa, B., Giguere, P.: Mixvpr: Feature mixing for visual place recognition. In: WACV, pp. 2998–3007 (2023)



- [4] Xu, S., Zhang, C., Fan, L., Meng, G., Xiang, S., Ye, J.: Addressclip: Empowering vision-language models for city-wide image address localization. In: ECCV (2024)
- [5] Achiam, J., Adler, S., Agarwal, S., Ahmad, L., Akkaya, I., Aleman, F.L., Almeida, D., Altenschmidt, J., Altman, S., Anadkat, S., et al.: Gpt-4 technical report. arXiv preprint arXiv:2303.08774 (2023)
- [6] Bai, J., Bai, S., Yang, S., Wang, S., Tan, S., Wang, P., Lin, J., Zhou, C., Zhou, J.: Qwen-vl: A versatile vision-language model for understanding, localization, text reading, and beyond. (2023)
- [7] Liu, H., Li, C., Wu, Q., Lee, Y.J.: Visual instruction tuning. In: NeurIPS (2024)
- [8] Yang, Z., Li, L., Lin, K., Wang, J., Lin, C.-C., Liu, Z., Wang, L.: The dawn of lmms: Preliminary explorations with gpt-4v (ision). arXiv preprint arXiv:2309.17421 **9**(1), 1 (2023)
- [9] Li, L., Ye, Y., Jiang, B., Zeng, W.: Georeasoner: Geo-localization with reasoning in street views using a large vision-language model. In: ICML (2024)
- [10] Hu, E.J., Shen, Y., Wallis, P., Allen-Zhu, Z., Li, Y., Wang, S., Wang, L., Chen, W.: Lora: Low-rank adaptation of large language models. arXiv preprint arXiv:2106.09685 (2021)
- [11] Durgam, A., Paheding, S., Dhiman, V., Devabhaktuni, V.: Cross-view geo-localization: a survey. arXiv preprint arXiv:2406.09722 (2024)
- [12] Torii, A., Sivic, J., Pajdla, T., Okutomi, M.: Visual place recognition with repetitive structures. In: CVPR, pp. 883–890 (2013)
- [13] Berton, G., Masone, C., Caputo, B.: Rethinking visual geo-localization for large-scale applications. In: CVPR, pp. 4878–4888 (2022)
- [14] Zhang, X., Wang, L., Su, Y.: Visual place recognition: A survey from deep learning perspective. Pattern Recognition **113**, 107760 (2021)
- [15] Hausler, S., Garg, S., Xu, M., Milford, M., Fischer, T.: Patch-netvlad: Multi-scale fusion of locally-global descriptors for place recognition. In: CVPR, pp. 14141–14152 (2021)
- [16] Keetha, N., Mishra, A., Karhade, J., Jatavallabhula, K.M., Scherer, S., Krishna, M., Garg, S.: Anyloc: Towards universal visual place recognition. IEEE Robotics and Automation Letters (2023)
- [17] Seo, P.H., Weyand, T., Sim, J., Han, B.: Cplanet: Enhancing image geolocalization by combinatorial partitioning of maps. In: ECCV, pp. 536–551 (2018)
- [18] Pramanick, S., Nowara, E.M., Gleason, J., Castillo, C.D., Chellappa, R.: Where

- in the world is this image? transformer-based geo-localization in the wild. In: ECCV, pp. 196–215 (2022)
- [19] Clark, B., Kerrigan, A., Kulkarni, P.P., Cepeda, V.V., Shah, M.: Where we are and what we’re looking at: Query based worldwide image geo-localization using hierarchies and scenes. In: CVPR, pp. 23182–23190 (2023)
  - [20] Trivigno, G., Berton, G., Aragon, J., Caputo, B., Masone, C.: Divide&classify: Fine-grained classification for city-wide visual geo-localization. In: ICCV, pp. 11142–11152 (2023)
  - [21] Radford, A., Kim, J.W., Hallacy, C., Ramesh, A., Goh, G., Agarwal, S., Sastry, G., Askell, A., Mishkin, P., Clark, J., *et al.*: Learning transferable visual models from natural language supervision. In: ICML, pp. 8748–8763 (2021)
  - [22] Haas, L., Alberti, S., Skreta, M.: Learning generalized zero-shot learners for open-domain image geolocalization. arXiv preprint arXiv:2302.00275 (2023)
  - [23] Cepeda, V.V., Nayak, G.K., Shah, M.: Geoclip: Clip-inspired alignment between locations and images for effective worldwide geo-localization. arXiv preprint arXiv:2309.16020 (2023)
  - [24] Touvron, H., Lavril, T., Izacard, G., Martinet, X., Lachaux, M.-A., Lacroix, T., Rozière, B., Goyal, N., Hambro, E., Azhar, F., *et al.*: Llama: Open and efficient foundation language models. arXiv preprint arXiv:2302.13971 (2023)
  - [25] Jiang, A.Q., Sablayrolles, A., Mensch, A., Bamford, C., Chaplot, D.S., Casas, D.d.l., Bressand, F., Lengyel, G., Lample, G., Saulnier, L., *et al.*: Mistral 7b. arXiv preprint arXiv:2310.06825 (2023)
  - [26] Yang, A., Yang, B., Hui, B., Zheng, B., Yu, B., Zhou, C., Li, C., Li, C., Liu, D., Huang, F., *et al.*: Qwen2 technical report. arXiv preprint arXiv:2407.10671 (2024)
  - [27] Abdin, M., Jacobs, S.A., Awan, A.A., Aneja, J., Awadallah, A., Awadalla, H., Bach, N., Bahree, A., Bakhtiari, A., Behl, H., *et al.*: Phi-3 technical report: A highly capable language model locally on your phone. arXiv preprint arXiv:2404.14219 (2024)
  - [28] Team, G., Anil, R., Borgeaud, S., Wu, Y., Alayrac, J.-B., Yu, J., Soricut, R., Schalkwyk, J., Dai, A.M., Hauth, A., *et al.*: Gemini: a family of highly capable multimodal models. arXiv preprint arXiv:2312.11805 (2023)
  - [29] Zhu, S., Yang, T., Chen, C.: Vigor: Cross-view image geo-localization beyond one-to-one retrieval. In: CVPR, pp. 3640–3649 (2021)
  - [30] Ghanem, A., Abdelhay, A., Salah, N.E., Nour Eldeen, A., Elhenawy, M., Masoud,

- M., Hassan, A.M., Hassan, A.A.: Leveraging cross-view geo-localization with ensemble learning and temporal awareness. *PloS one* **18**(3), 0283672 (2023)
- [31] Wang, T., Zheng, Z., Yan, C., Zhang, J., Sun, Y., Zheng, B., Yang, Y.: Each part matters: Local patterns facilitate cross-view geo-localization. *IEEE Transactions on Circuits and Systems for Video Technology* **32**(2), 867–879 (2021)
- [32] Mi, L., Xu, C., Castillo-Navarro, J., Montariol, S., Yang, W., Bosselut, A., Tuia, D.: Congeo: Robust cross-view geo-localization across ground view variations. *arXiv preprint arXiv:2403.13965* (2024)
- [33] Hao, X., Chen, W., Yan, Y., Zhong, S., Wang, K., Wen, Q., Liang, Y.: Urban-ulp: A multi-granularity vision-language pre-trained foundation model for urban indicator prediction. *arXiv preprint arXiv:2403.16831* (2024)
- [34] Contributors, X.: XTuner: A Toolkit for Efficiently Fine-tuning LLM. <https://github.com/InternLM/xtuner> (2023)
- [35] Lin, J., Yin, H., Ping, W., Molchanov, P., Shoeybi, M., Han, S.: Vila: On pre-training for visual language models. In: *CVPR*, pp. 26689–26699 (2024)
- [36] Claude: The claude 3 model family: Opus, sonnet, haiku. (2024). <https://api.semanticscholar.org/CorpusID:268232499>
- [37] Qwen: Qwen2-vl (2024)